Proc. Natl. Acad. Sci. USA
Vol. 89, pp. 3473–3477, April 1992
Medical Sciences

In situ optical histochemistry of human artery using near infrared Fourier transform Raman spectroscopy

JOSEPH J. BARAGA*†, MICHAEL S. FELD*, AND RICHARD P. RAVA*‡

*George R. Harrison Spectroscopy Laboratory and †Division of Health Sciences and Technology, Massachusetts Institute of Technology, Cambridge, MA 02139

Communicated by Britton Chance, January 2, 1992 (received for review June 6, 1991)

ABSTRACT **In this paper we demonstrate that near infrared Fourier transform Raman spectroscopy provides unprecedented biochemical information about the extent of atherosclerosis in human aorta. In particular, elastin, collagen, cholesterol, cholesterol esters, lipids, carotenoids, and calcium apatite deposits all can be discerned by using this technique, permitting study of each stage in the disease process. Additionally, these moieties can be detected over 1.5 mm below the irradiated surface of the tissue, possibly allowing extraction of three-dimensional information about the histology of atherosclerotic plaques. We propose that this technique may be utilized for *in situ* optical histochemical analysis of atherosclerosis in particular and human disease in general.**

The role of the pathologist is to determine and understand the microscopic structural and functional changes in tissue that are caused by or effectuate a disease. By utilizing biopsy samples, the pathologist will diagnose a malady by employing histochemical means to scrutinize the tissue. In certain instances, however, it may be impossible to remove small amounts of tissue for examination, or the anatomical manifestations of the disorder are ambiguous so that diseased regions cannot be reliably identified for biopsy. In these cases, an *in situ* technique that can rapidly provide information similar to that available from histochemical examinations of biopsy specimens would be of significant value.

In a search for *in situ* methods, several groups have looked to optical spectroscopy, almost exclusively in the form of fluorescence emission, for diagnosis of disease (1). Optical systems provide access to many organs in the body with the use of flexible optical fibers to excite and collect the spectroscopic signals, and high-performance diagnoses for several pathologic conditions have been demonstrated (1). However, detailed biochemical information, suitable for histochemical analysis of the tissue, is not available by using fluorescence techniques. In this report we demonstrate that near infrared (NIR) Fourier transform (FT) Raman spectroscopy (2) can be utilized as an *in situ* optical probe of disease, providing histochemical information unparalleled by other optical methods. In addition, we will show that the spectra reflect the chemical state of the tissue up to 1.5 mm below the irradiated surface, possibly permitting three-dimensional information to be obtained.

As an example of the promise of this approach, we have chosen the disease atherosclerosis for initial study. In the United States, myocardial infarctions, almost entirely attributable to coronary artery atherosclerosis, account for 20–25% of all deaths (3). Although several therapies are available for treatment of atherosclerosis, no reliable methods can predict in advance which lesions will progress despite a particular medical therapy (4). One major reason is that *in situ* biopsy of blood vessels is very difficult, and so histopathology cannot be used to provide detailed information about the state of the diseased vessel or to scrutinize the pathogenesis *in vivo*.

The mechanism of atherogenesis is not yet fully understood; however, the biological stages are beginning to be elucidated (5). The initiating step appears to be a breakdown in the integrity of the endothelial layer of the vessel, which permits infiltration of low density lipoproteins containing cholesterol. This insult can lead to denudation of the endothelial layer, resulting in platelet aggregation at the intima surface and release of platelet growth factors. Arterial smooth muscle cell and connective tissue proliferation as well as monocyte infiltration into the intima commences to repair the injury. Cells take up the cholesterol-rich lipoproteins to become foam cells. As the lesion progresses, the cycle is repeated with old foam cells necrosing and localizing to the bottom of the lesion, near the internal elastic lamina, and becoming supersaturated with cholesterol (6). The buildup of necrotic material and mineralization in the form of calcium apatite crystallization leads to complicated advanced atheromas with hemodynamically important implications.§

In this paper, we show that NIR FT Raman spectroscopy can probe many of the molecules that are important in the formation of an advanced atherosclerotic lesion. After a review of the experimental protocol in the following section, the FT Raman spectra of several histologically distinct lesions are presented. Possible applications of this method to the study of atherogenesis and the guidance of different treatment modalities are then discussed.

METHODS

FT Raman spectra were measured from 0 to 4000 cm^{-1} with a Perkin-Elmer model 1760X FT-IR spectrometer equipped with a Perkin-Elmer FT Raman accessory (7). The accessory employs a 180° backscattering geometry and a cooled (77 K) InGaAs detector. A 1064-nm continuous wave Nd:YAG laser was used for irradiating samples with 500-mW laser power in a 1.0-mm diameter spot at the sample. An additional Raman

The publication costs of this article were defrayed in part by page charge payment. This article must therefore be hereby marked "*advertisement*" in accordance with 18 U.S.C. §1734 solely to indicate this fact.

Abbreviations: NIR, near infrared; FT, Fourier transform.

‡To whom reprint requests should be addressed.

§Normal human artery is composed of three distinct layers: intima, media, and adventitia. The intima, normally 50–300 μm thick depending on the artery, is the innermost layer. It is mainly composed of collagen fibers and ground substance primarily formed from proteoglycans (3). A single layer of endothelial cells in the vessel lumen protects the intima from injury. The media, several hundred micrometers thick, can be quite elastic or muscular depending on the artery. The structural protein elastin is the major component of aortic media, whereas smooth muscle cells make up the majority of the media in coronary artery. The outermost adventitial layer serves as a connective tissue network, which loosely anchors the vessel in place, and is mainly made up of lipids, lipoproteins, and collagen. During the atherosclerotic process, the intima thickens due to collagen accumulation and smooth muscle cell proliferation, lipid and necrotic deposits accumulate under and within the collagenous intima, and eventually, calcium builds up, leading to calcium apatite deposits in the artery wall.

edge filter (Physical Optics) was utilized to remove completely the large Rayleigh scattering from the tissue in order to collect Raman data. Two successive spectra were obtained from each sample, and no sample degradation was observed under the experimental conditions.

Human aorta was chosen for initial study as an instance of atherosclerotic artery tissue. Samples were obtained at the time of postmortem examination, rinsed with isotonic saline solution (buffered at pH 7.4), snap-frozen in liquid nitrogen, and stored at −85°C until use. Prior to spectroscopic study, samples were passively warmed to room temperature while being kept moist with the isotonic saline. Normal and atherosclerotic areas of tissue were identified by gross inspection, separated, and sliced into roughly 8 × 8 mm pieces. The tissue samples were placed in a suprasil quartz cuvette with a small amount of isotonic saline to keep the tissue moist and with one surface in contact with the window irradiated by the laser. A total of 51 specimens from 19 patients were studied. The spectra shown in this paper were collected with 512 scans at 8-cm^{-1} resolution (≈35-min total collection time). After spectroscopic examination, all specimens were histologically analyzed to verify the gross identifications.

RESULTS

Normal Aorta NIR FT Raman Spectrum. A typical NIR FT Raman spectrum from normal aorta is shown in Fig. 1. When irradiated from the intimal side (Fig. 1, spectrum a), the major vibrational bands observed in normal aorta are all attributable to protein vibrations: the band at 1658 cm^{-1} is assigned to the amide I vibration of the polypeptide chain, the 1453-cm^{-1} band is assigned to a C—H bending mode of proteins, and the 1252-cm^{-1} band is assigned to the amide III vibration (8). The spectrum of normal aorta is at least 25% weaker than any of the pathologic samples. The peak frequency of the C—H bending band, which averaged 1451 ± 1 cm^{-1} for all the normal specimens, is specific to the protein C—H bending mode (see below). The weak band near 1335 cm^{-1}, which appears as a shoulder in many of the normal specimens, appears to be specific to elastin, and the weak band at 1004 cm^{-1} is likely due to phenylalanine residues. In general, the relative intensities of the bands in the region between 1250 and 1340 cm^{-1} appear very much like those observed in the FT Raman spectrum of elastin (9). This observation is consistent with the thin collagenous intima in normal aorta, the elastic nature of the media of aorta, and the deep penetration depth of 1064-nm radiation. Band assignments for all tissue types are listed in Table 1.

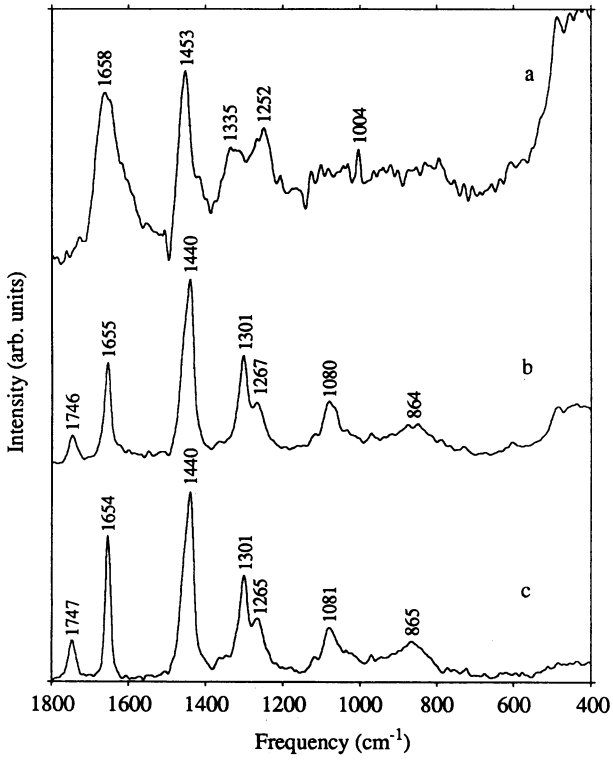

FIG. 1. NIR FT Raman spectra from normal aorta irradiated from the intimal side (spectrum a) or irradiated from the adventitial side (primarily adipose tissue) (spectrum b). NIR FT Raman spectrum of the triglyceride, triolein, is shown in spectrum c. The amplitude of the intimal Raman spectrum (spectrum a) has been expanded by a factor of 3 relative to that in spectra b and c.

Spectrum b in Fig. 1 displays the NIR FT Raman spectrum of the adventitial side of normal aorta. In this case, the irradiated adventitial surface consisted of several millimeters of visible adipose tissue. In contrast with the spectrum collected from the intimal side, the bands observed in this adipose material appear to be mainly due to lipid, and in particular to triglyceride, with almost no contribution from protein. This is not unexpected, as the triglyceride content of adipose tissue is on the order of 60%. The sharp band at 1655 cm^{-1} is due to stretching of C=C groups in unsaturated fatty acid chains. This band is distinguished from amide I by its peak frequency and its width, which in this case is 17 cm^{-1} full width at half-maximum. Amide I, in contrast, is ≈60 cm^{-1} wide. The dominant C—H bending band is shifted to 1440 cm^{-1}, which is characteristic of lipids. This band is about 3 times more intense in adipose tissue than in normal intima, probably a result of the greater number of C—H groups per unit volume in triglycerides. The bands at 1301/1267 cm^{-1} and 1080 cm^{-1} are assigned to C—H bending and C—C stretching vibrations of fatty acids, respectively.

The 1746-cm^{-1} band, assigned to the C=O stretching mode of the triglyceride ester linkages, indicates that most of the lipid observed in the adventitial adipose tissue is of the triglyceride form. Specifically, the integrated intensity of this band relative to the C—H bending band at 1440 cm^{-1} is equal to 0.103, whereas this same ratio for triolein is 0.136, which indicates that ≈75% of the C—H band is due to triglyceride. The NIR FT Raman spectrum of triolein (a triglyceride containing fatty acid chains of 18 carbons and a single double bond) is shown for comparison in Fig. 1, spectrum c. Additional molecular information regarding the state of the fatty acid chains is readily deduced from the adventitial adipose spectrum. For example, the relative intensity of the C=C band at 1655 cm^{-1} indicates that there are on average ≈0.7 unsaturated double bonds per fatty acid chain, assuming fatty acids of 16–18 carbons. In addition, the frequencies and structures of the C—H bending and C—C stretching bands suggest that most of the fatty acid chains are in the gauche conformation. The sharp 1129-cm^{-1} band, characteristic of all-trans chains, is not observed in the spectrum.

Fibrous and Atheromatous Plaques NIR FT Raman Spectra. The NIR FT Raman spectra of fibrous plaque specimens exhibit a range of features. Fig. 2, spectrum a shows a representative spectrum from one of the types of fibrous plaques. These fibrous plaque spectra are quite similar in both relative and absolute band intensities to the spectra of normal aorta. The most significant differences are that the C—H bending band, peaking near 1448 cm^{-1} on average, is shifted by 3 cm^{-1} to a slightly lower frequency. This may be the result of a small increase in the lipid content of these plaques relative to normal aorta. In addition, the band near 1340 cm^{-1}, attributed to elastin in normal aorta, is decreased relative to amide III at 1265 cm^{-1}. The putative explanation is that the collagenous intima (13) is thickened in these specimens, so that the spectral contribution from the elastic media is reduced relative to that of normal aorta.

Table 1. Peak frequencies of selected bands in normal and atherosclerotic aorta

Aorta sample						
Normal	Adventitia	Fibrous plaque	Fatty plaque	Exposed calcif. I	Exposed calcif. II	Assignment (ref.)
	1746w					C=O (ester) stretch
		1667m	1667m		1667m	C=C stretch of lipid
1658s				1663m		Amide I (8)
	1655m					C=C stretch of fatty acids
		1519w				Carotenoid (10)
						C—H bend (8)
1451s				1450s		Protein
	1440s	1440s	1440s		1440s	Lipid
	1301m	1301w	1301w		1300w	Lipid C—H bend (CH_2)
	1267w	1264w	1262w		1262w	Lipid C—H bend (=C—H)
1252m				1261w		Amide III (8)
		1157w				Carotenoid (10)
		1131w	1130w	1128w		C—C stretch of lipid
	1080m	1086w	1088w			
						Carbonate symmetric and phosphate antisymmetric
				1071s	1071s	stretch in calcium salts (11)
1004w		1004w	1004w			Phenylalanine (8)
						Phosphate symmetric stretch in
				960vs	960vs	calcium salts (11)
		957w	959w			Cholesterols (12)
		882w	882w		878w	Cholesterols (12)
		842w	841w		850w	Cholesterols (12)
		803w	801w		804w	Cholesterols (12)
		700m	700m		699m	Cholesterols (12)
		606w	606w			Cholesterols (12)
		546w	546w		547w	Cholesterols (12)
				587m	587m	Phosphate in calcium salts (11)

Peak frequencies of typical specimens, accurate to ±1 cm^{-1}. vs, Very strong; s, strong; m, medium; and w, weak relative band intensity. Calcif., calcification.
*Adventitia specimen is mainly adipose tissue.

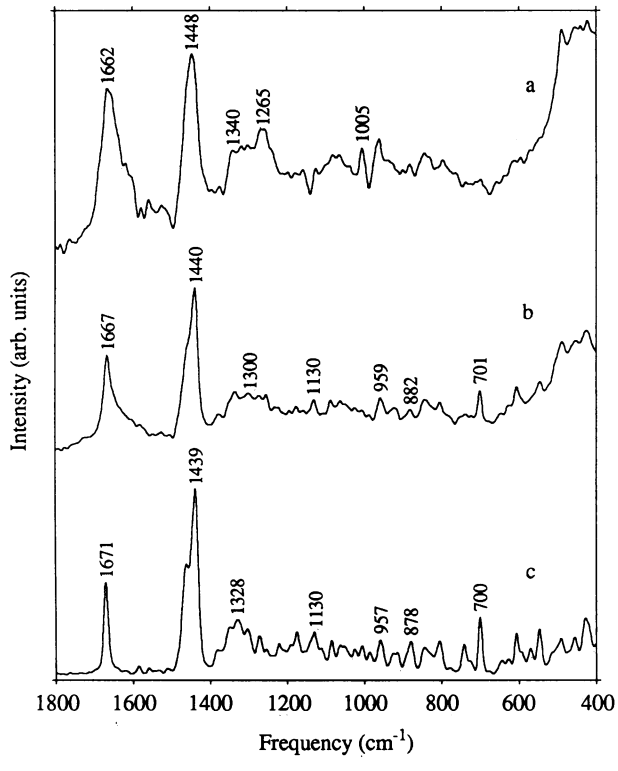

FIG. 2. NIR FT Raman spectra from a fibrous plaque (spectrum a), an atheromatous plaque (spectrum b), and a cholesterol monohydrate powder (spectrum c).

The NIR FT Raman spectra of other fibrous plaque specimens appeared similar to spectra of atheromatous plaques (Fig. 2, spectrum b). These are substantially different than either normal aorta or adipose tissue. In these cases, the intense C—H bending band occurs at 1440 cm^{-1}, characteristic of lipid material. This band is roughly twice as intense as the C—H bending band in normal aorta. The complete absence of a band at 1746 cm^{-1} indicates that this lipid is not a triglyceride. In fact, this lipid appears to be predominantly cholesterols, as identified by the sharp, characteristic band at 700 cm^{-1} and comparison to the cholesterol spectrum shown in Fig. 2, spectrum c (12). Again, this is not surprising, since cholesterols accumulate in high concentrations in atherosclerotic lesions (6). Several of the bands between 1000 and 500 cm^{-1} are assignable to vibrational modes of the sterol rings. These include the bands at 959, 882, 844, 805, 700, 605, and 546 cm^{-1}. In addition, the 1667-cm^{-1} band is attributed in part to the C=C stretching vibration of the steroid nucleus.

The presence of fatty acid chains in the atheromatous plaque spectra is evidenced by bands at 1300/1262 cm^{-1} and 1130/1088 cm^{-1}, due to C—H bending and C—C stretching vibrations, respectively. These bands may contain contributions from cholesterol as well. The relative intensities of the fatty acid band at 1300 cm^{-1} and the sterol ring bands suggest a mixture of free cholesterol and cholesterol fatty acid esters. Moreover, the relative intensities of the 1130 cm^{-1} C—C stretching and the 700 cm^{-1} sterol bands indicate that most of the fatty acid chains are in the gauche conformation, consistent with the predominance of unsaturated fatty acid chains in the cholesterol esters in these plaques. It is particularly noteworthy in the atheromatous plaques that the cholesterol deposits are detected from material *below a thick*

fibrous cap, indicating the ability of the NIR FT Raman method to probe materials several hundred micrometers below the tissue surface.

In addition to the cholesterol and cholesterol ester bands, the NIR FT Raman spectra of some of the fibrous plaques contained unique bands at 1519 and 1157 cm^{-1}. The intensities of these bands are highly correlated, which suggests that they are due to a single component. These bands, which have been previously observed in visibly excited Raman spectra of atherosclerotic plaques, are assigned to carotenoids (10, 14). The amount of carotenoid in these plaques is probably much smaller than the amount of cholesterols or proteins, but may be strongly preresonance enhanced (15). The carotenoid bands are observed only in this subset of fibrous plaques.

Calcified Plaques and Exposed Calcifications NIR FT Raman Spectra. The NIR FT Raman spectrum of calcified plaque, containing a subsurface calcified deposit and an overlying soft fibrous cap, exhibits an intense, sharp, new band at 960 cm^{-1} (Fig. 3, spectrum a). This band, specific to calcified tissue, is assigned to the symmetric stretching vibration of phosphate groups (11), which are present in high concentrations in the solid calcium salts. The weaker phosphate antisymmetric stretch is also present at 1072 cm^{-1}. A symmetric stretching vibration of carbonate groups may also contribute to this latter band. The phosphate vibrations are easily observed from subsurface deposits in the calcified plaques; the 960 cm^{-1} band can be observed from deposits up to 1.5 mm beneath a soft tissue cap with the current signal-to-noise level (see below). The calcified plaque also displays protein vibrations from the fibrous tissue cap. These include amide I at 1664 cm^{-1} and amide III near 1257 cm^{-1}. The C—H bending band at 1447 cm^{-1} suggests a mixture of protein and lipid, and the weak band at 699 cm^{-1} is likely due to cholesterol that is either in the fibrous cap, the calcified deposit, or both.

The NIR FT Raman spectra of exposed calcifications (Fig. 3, spectrum b) display a range of features. In all cases, the major bands are due to the calcium salts. These include the 960-cm^{-1} phosphate and 1072-cm^{-1} phosphate/carbonate bands as well as the band at 587 cm^{-1}, which is assigned to another phosphate vibrational mode. On the other hand, several differences are apparent in the weaker bands, which are presumably due to soft tissue components that are embedded in the calcification. In some cases (data not shown), the C—H bending band occurs at 1450 cm^{-1}, and the band at 1663 cm^{-1} is similar in shape to amide I for some of the calcifications, which is indicative of protein vibrational modes. In other calcified plaques, such as that in Fig. 3, spectrum b, the C—H bending band occurs at 1440 cm^{-1}, and the 1667-cm^{-1} band, which is much sharper, is more likely due to C=C stretching vibrations. In this plaque, the bands are due to lipid, in particular cholesterols, as evidenced by the 700-cm^{-1} and 1300-cm^{-1} bands.

In our histological examinations of aorta, two distinct types of exposed calcifications have been noted. In one type, the fibrous tissue cap is calcified. In the other, the necrotic core of an atheromatous plaque is calcified, and the calcified deposit is exposed by ulceration of the soft tissue fibrous cap. A possible explanation for the two spectral types of exposed calcifications is that the specimens that exhibit protein bands are of the former histologic type, whereas the specimens that exhibit lipid bands are of the latter type.

NIR Radiation Raman Probe Depths. With the observation that several of the biochemical species important in the atherosclerotic process, including cholesterol and calcium hydroxyapatite, can be easily detected below the tissue surface, we wished to determine the depth limit of detection using the NIR FT Raman technique. To address this question, ten 200-μm sections of aortic media were cut and placed one at a time over a large calcified deposit (6 × 6 × 3 mm), and the FT Raman spectra at the 960-cm^{-1} band were monitored as a function of depth below the surface. As indicated by the plot of FT Raman intensity versus depth shown in Fig. 4, the signal from the calcified deposit was detectable until the deposit was greater than 1.6 mm below the irradiated surface. Even slightly deeper depths could be probed if the focus of the collection optics was moved into the tissue.

The two-dimensional resolution of the NIR FT Raman signal for materials below the tissue surface was then tested by placing 1 mm of aortic media above another calcified deposit and moving the tissue transversely in two dimensions through the laser beam and collection lens. The FT Raman

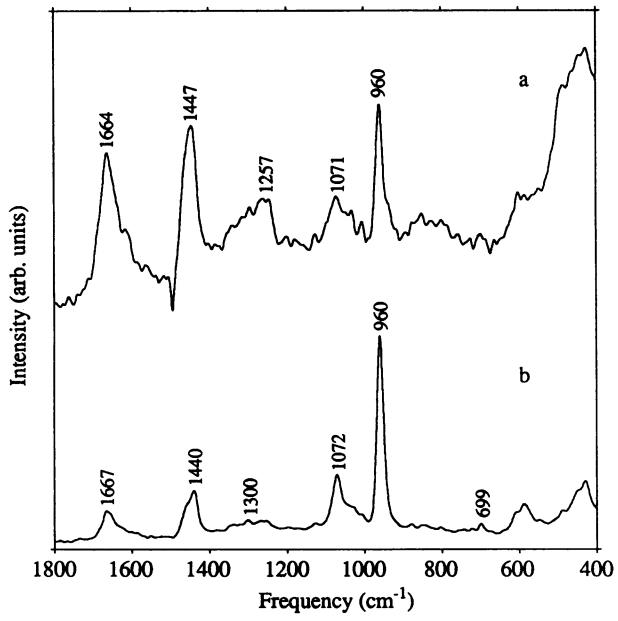

FIG. 3. NIR FT Raman spectra from calcified plaque (with a fibrous cap) (spectrum a) and exposed calcification (spectrum b). The amplitude of the calcification with a fibrous cap Raman spectrum (spectrum a) has been expanded by a factor of 8 relative to that in spectrum b.

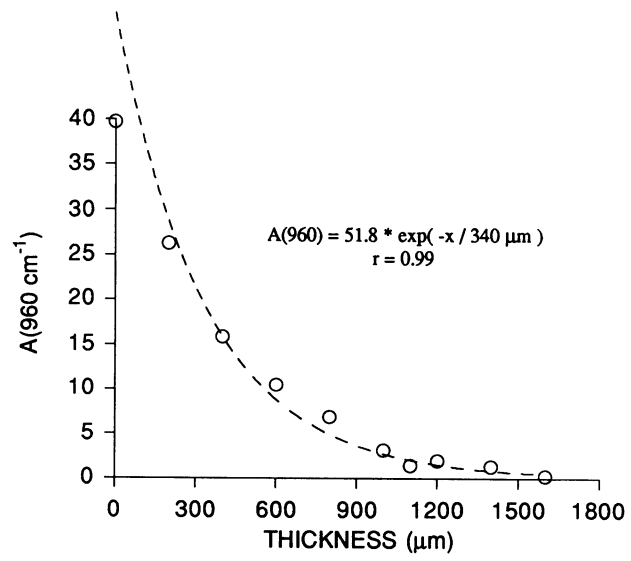

FIG. 4. Measured NIR Raman intensity of the 960-cm^{-1} band [A(960 cm^{-1}) indicates the area of this band] in a calcified deposit as a function of depth below the irradiated surface. The dashed curve corresponds to the fit of an exponential function to the data with an exponent of 2.94 mm^{-1}.

signal was observed to drop off rapidly as the beam and collection optics moved from the calcified deposit. The detected FT Raman signal closely followed the geometry of the calcified deposit below the surface, despite the significant scattering of the overlying layer of tissue. This result suggests that the Raman scattered light may be utilized for imaging objects below the tissue surface with minimal image blurring due to elastic scattering in the tissue.

DISCUSSION

Currently available diagnostic modalities for atherosclerosis primarily rely on the detection of structural and/or morphologic changes in the artery wall. Examples of these techniques include angiography, angioscopy, ultrasound, and magnetic resonance imaging (3). While these methods can provide clinically useful information about the anatomic alterations in the arterial wall due to atherosclerotic lesions, they cannot provide the biochemical or molecular information that might be utilized to guide treatment or study the disease progression. Such histochemical information is generally provided only from biopsy tissue and chemical staining techniques (3).

Previous attempts to obtain Raman spectra from cardiovascular tissue by using visible excitation suffered somewhat from fluorescence interference, although the vibrations from carotenoids were detected in plaques, and calcium apatite vibrations could be discerned in calcified tissue (16, 17). NIR FT Raman of aorta reported by us in an earlier note (18) and in this paper offers several advantages over visibly excited Raman spectroscopy. The NIR excitation avoids the fluorescence interference inherent in visible Raman spectra of tissue as well as the photolytic decomposition that can take place. In addition, the Fourier instrument offers high throughput (Jacquinot and multiplex advantage) for rapid data collection and frequency precision for searching for small but important shifts in the Raman spectra of biological systems. Finally, the deep penetration depth of NIR excitation allows detection of subsurface alterations in the artery wall.

To our knowledge, the NIR FT Raman data provided in this paper demonstrate the first *in situ* optical method that may be able to probe the early histochemistry of the atherosclerotic process. In particular, the detection of cholesterol and the ability to differentiate its chemical state from other lipids may allow *in vivo* determination of atherosclerotic plaque histochemistry. Similarly, the detection of subsurface cholesterol and calcium apatite deposits in conjunction with other observed variations for different stages of atherogenesis should permit study of disease progression as well as response to divergent treatment modalities. Finally, the sharp discrimination of the FT Raman signal with mechanical scanning of the laser and collection optics across the tissue, when coupled with triangulation information from FT Raman collection at additional angles, might enable three-dimensional imaging of 1.5–2.0 mm of tissue, a dimension equivalent to the width of a typical coronary artery.

Such information may allow for real time determination of the correct treatment modality for different atherosclerotic lesions. For example, the physician could determine the composition of a lesion and then may be able to decide whether balloon angioplasty or laser therapy was indicated. In the case of the latter, NIR FT Raman provides the ultimate guidance system, offering not only unambiguous diagnostic capabilities but also the ability to detect the adventitia while still greater than 1.5 mm from the outer surface and thus completely avoid vessel wall perforation.

CONCLUSIONS

We have shown that NIR FT Raman spectra of human aorta provide important information concerning the histochemistry of artery and progression of atherosclerosis. In particular, elastin, collagen, lipids, carotenoids, cholesterol, and calcium apatite deposits can be discerned by using this technique, permitting a study of each stage in the disease process. Both the ability to observe these materials up to 1.5 mm below the tissue surface and the observation that the detected NIR Raman signals closely follow the geometry of the deposit, even when the material is below the tissue surface, indicate that biochemically based three-dimensional imaging may be possible with NIR Raman techniques. We believe that NIR Raman spectroscopy will become an important tool in both the clinical pathology and histochemical analysis of atherosclerosis in particular and human disease in general.

We are actively pursuing the extension of NIR Raman spectroscopy to the clinical setting. Implementation of new technology (19), such as CCD (charge coupled device) array detection with 800- to 900-nm excitation, is required to provide high-quality Raman signals through optical fibers in real time as is mandatory for human *in vivo* work. We have obtained preliminary results indicating the applicability of this technology to the study of arterial disease (20).

We wish to thank Dr. R. Manoharan for helpful discussions concerning the NIR Raman spectra of different biological constituents and the preresonance enhancement of the carotenoid NIR FT Raman signal. Vinny Moylan, Mark Knowlton, and Connie Austin of the Brigham and Women's Hospital in Boston are gratefully acknowledged for providing arterial samples. This work was completed at the National Institutes of Health-supported Massachusetts Institute of Technology Laser Biomedical Research Center (National Institutes of Health Grant RR02594).

1. Richards-Kortum, R., Rava, R. P., Fitzmaurice, M., Tong, L. L., Ratliff, N. B., Kramer, J. R. & Feld, M. S. (1989) *IEEE Trans. Biomed. Eng.* **36**, 1222–1232.
2. Hirschfeld, T. & Chase, B. (1986) *Appl. Spectrosc.* **40**, 133–139.
3. Cortran, R. S., Kumar, V. & Robbins, S. L. (1989) *Pathologic Basis of Disease* (Saunders, Philadelphia).
4. Ellis, S. G., Roubin, G. S., King, S. B., Douglas, J. S. & Cox, W. R. (1989) *Am. J. Cardiol.* **63**, 30–34.
5. Steinberg, D. (1988) *Atheroscler. Rev.* **18**, 1–23.
6. Small, D. M. (1988) *Arteriosclerosis* **8**, 103–129.
7. Cutler, D. J. (1990) *Spectrochim. Acta part A* **46**, 131–151.
8. Carey, P. R. (1982) *Biochemical Applications of Raman and Resonance Raman Spectroscopies* (Academic, New York).
9. Frushour, B. G. & Koenig, J. L. (1975) *Biopolymers* **14**, 379–391.
10. Barnes, M. J. (1985) *Collagen Relat. Res.* **5**, 65–97.
11. Faiman, R. (1977) *Chem. Phys. Lipids* **18**, 84–104.
12. Sufra, S., Dellepiane, G., Masetti, G. & Zerbi, G. (1977) *J. Raman Spectrosc.* **6**, 267–271.
13. Blankenhorn, D. H. (1960) *Ann. Intern. Med.* **53**, 944–954.
14. Bennett, R., Cutler, D. J., Mould, H. M. & Chapman, D. (1990) *J. Raman Spectrosc.* **21**, 699–702.
15. Nelson, D. G. A. & Wiliamson, B. E. (1982) *Aust. J. Chem.* **35**, 715–727.
16. Clarke, R. H., Wang, Q. & Isner, J. M. (1988) *Appl. Opt.* **27**, 4799–4800.
17. Clarke, R. H., Hanlon, E. B., Isner, J. M. & Brody, H. (1987) *Appl. Opt.* **26**, 3175–3177.
18. Rava, R. P., Baraga, J. J. & Feld, M. S. (1991) *Spectrochim. Acta Part A* **47**, 509–512.
19. Allred, C. D. & McCreery, R. L. (1990) *Appl. Spectrosc.* **44**, 1229–1231.
20. Baraga, J. J., Field, M. S. & Rava, R. P. (1992) *Appl. Spectrosc.* **46**, 187–190.